MULTI-FRAME MOTION ESTIMATION FOR FREEHAND ELASTOGRAPHY AND ITS APPLICATION TO THYROID TUMOR IMAGING

Adrian Basarab[1], Andrej Lyshchik[2], Philippe Delachartre[1]

CREATIS-LRMN, CNRS UMR 5520, INSERM U630, INSA-Lyon, F-69621, France[1], Department of Radiology and Radiological Sciences, Vanderbilt University Medical Center, USA[2]

ABSTRACT

In this study we investigated multi-frame motion estimation for freehand ultrasound elastography and its application to thyroid tumor imaging. Motion analysis using a technique of compression orientation detection led us to introduce a new parameter based on the angle of estimated motion vectors. We show how our method may improve the quality of the results compared to classical strain images.

Index Terms— multi-frame motion estimation, ultrasound elastography, image registration.

1. INTRODUCTION

Among motion estimation techniques, those based on block matching [1] are the most common and have their application in different fields, such as moving picture coding or medical domain. In ultrasound imaging, one of the medical applications for motion tracking is elastography [2]. The basis of this method lies in the significant difference in the elastic properties between normal and diseased tissues, in our case between normal thyroid and malignant thyroid tumors [3]. It consists in measuring the elasticity of soft tissues, using ultrasound images acquired while a compressive force is freehandly applied to the tissue surface, directly with the ultrasound probe. First, motion tracking between images acquired in this way is processed. The estimated motion is then used to reconstruct mechanical properties of the examined tissues. Usually, strain images calculated by derivation of the estimated displacement are shown.

Theoretically, all existing techniques of motion tracking can be used to estimate the displacement between ultrasound images. However, Yeung et al. show in [4] the challenges in motion tracking introduced by ultrasound images, such as speckle decorrelation and low signal-to-noise ratio. Moreover, the freehand compression does not allow any control of the tissues displacement. Therefore, estimation methods adapted to ultrasound images and more particularly to ultrasound elastography were proposed [5].

We have already presented in [6] a block matching based method using a bilinear parametric model to locally control the tissue deformation. Thus, we showed how the proposed multi-scale approach allows locally estimating small motions compared to the images resolution. We have also showed on simulated and in-vivo ultrasound images that this motion estimation method is more accurate than classical block matching. In this paper, we show how this motion tracking is expanded to multi-frame motion estimation. Compression orientation detection is proposed and shown to be a good criterion of eliminating *bad* images from an acquired sequence. Once the 2-D dense motion field estimated, a novel parameter is proposed and shown to improve image quality and resolution of thyroid elastograms compared as to classical strain images.

2. METHOD

2.1. Local motion modeling

The problem addressed here is to estimate the motion given a sequence of N ultrasound images, noted $I(x,y,t)$. The relation between a pair of consecutive frames is given in (1).

$$I(x,y,t+1) = I(x+u(x,y,t), y+v(x,y,t), t) \quad (1)$$

where $u(x,y,t)$ and $v(x,y,t)$ are the spatially varying motion fields along the two directions of the images (x and y are respectively the lateral and axial directions) between images t and $t+1$. Our method will independently estimate these two components in each pixel of the reference image t, for t running from 1 to $N-1$. Then, a global 2-D motion field is calculated in each pixel of image $I(x,y,1)$, taking into account the $N-1$ estimations done previously, as shown in figure 1 [7]. This strategy of estimation allows compression orientation estimation at each step in the sequence, as shown in section 2.3.

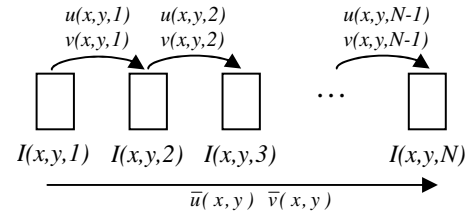

Figure 1. Schematic multi-frame motion tracking

2.2. Algorithm description

1. For each pair of images $I(x,y,t) \rightarrow I(x,y,t+1)$, do steps from 2 to 7.
Estimation between two images:
2. Create initial rectangular mesh on $I(x,y,t)$.
3. Define rectangular regions of interest around each node.
4. For each node, do steps 5 and 6.
Node *N:*
5. Estimate the parameters of the bilinear model (2) for the current region of interest.

$$\begin{cases} u(x,y,t) = a_u.x + b_u.y + c_u.x.y + d_u \\ v(x,y,t) = a_v.x + b_v.y + c_v.x.y + d_v \end{cases} \quad (2)$$

6. If final node, go to step 7, otherwise go to step 4.
7. Using the estimation result for all regions of interest, compute the dense motion field and make $t = t + 1$. If $t = N - 1$, go to step 8, otherwise go to step 1.
Calculate the global motion field $\bar{u}(x,y)$ and $\bar{v}(x,y)$:
8. Using the estimated motion between couples of images, we calculate for each of these couples two parameters giving an indication on how the compression have been applied between these images. For more details, see section 2.3.
9. Using the parameters calculated at step 8, we eliminate *bad* image couples. Let T be a vector containing the instants t which are not eliminated.
10. Transform the estimated displacements at each instant t so that the motion vectors correspond to the pixels of the first image $I(x,y,1)$. We obtain in this way the trajectory of all pixels of the first image along the image sequence. Let us denote by $u_t(x,y)$ and $v_t(x,y)$ the motion components between images $I(x,y,t)$ and $I(x,y,t+1)$ corresponding to pixels of frame $I(x,y,1)$. Obviously, for t equal to 1, we have:

$$u_1(x,y) = u(x,y,1) \quad and \quad v_1(x,y) = v(x,y,1) \quad (3)$$

Moreover, for t larger than 1, we have:

$$\begin{aligned} u_t(x,y) &= u\left(x + \sum_{j=1}^{t-1} u_j(x,y), y + \sum_{j=1}^{t-1} v_j(x,y), t\right) \\ v_t(x,y) &= v\left(x + \sum_{j=1}^{t-1} u_j(x,y), y + \sum_{j=1}^{t-1} v_j(x,y), t\right) \end{aligned} \quad (4)$$

11. Final global motion of sequence I is defined as:

$$\begin{aligned} \bar{u}(x,y) &= \frac{1}{card(T)} \sum_{j=1}^{card(T)} u_{T(j)}(x,y) \\ \bar{v}(x,y) &= \frac{1}{card(T)} \sum_{j=1}^{card(T)} v_{T(j)}(x,y) \end{aligned} \quad (5)$$

12. Calculate the motion ratio image (6) between the lateral and axial components of the estimated global motion. The relevance of this parameter for malignant tumors discrimination is discussed in section 4.

$$\frac{\bar{u}(x,y)}{\bar{v}(x,y)} = tan(\bar{\gamma}(x,y)) \quad (6)$$

where $\bar{\gamma}(x,y)$ is the orientation angle map of global motion vectors reported to the first selected image.

2.3. Compression orientation

As explained in the introduction, the motion we are estimating is the result of a freehand compression induced to the tissues directly by the ultrasound probe. Along an image sequence, the compression is not constant and can be very difficultly controlled. Therefore, we introduce a criterion in order to eliminate the images which are not coherent with the other frames in terms of applied compression. This criterion is used at steps 8 and 9 in the algorithm description above.
Figure 2 shows the conditions of acquisition for ultrasound elastography. We can observe that the compression is not necessarily axial, but can have an oblique orientation. In order to estimate this orientation, for each lateral profile (at depth y_0) of the lateral displacement map, we detect the lateral position x_0 as shown in (7).

$$x_0(t) = \arg\min_x(|u(x,y_0,t)|) \quad (7)$$

Thus, for a given estimation at an instant t, for each depth y_0 we find x_0 which represents the point that have the smallest lateral displacement. Points (x_0,y_0) are considered to belong to the compression orientation line shown in figure 2. As in an experimental case these points do not describe a perfect line, a first order polynomial function is fitted to this data in order to approximate the compression orientation, as shown in equation (8).

$$x_0 = y_0 \cdot tan(\gamma) + \delta \quad (8)$$

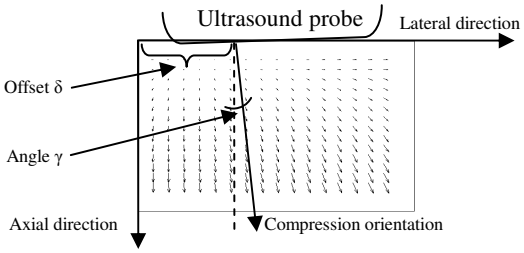

Figure 2. Schematic representation of the compression applied with the ultrasound probe.

The relevance of this approach is shown by the simulation result in the next section.

3. SIMULATION RESULTS

We present in this section a simulation result in order to validate the method of compression orientation detection explained previously. We used an experimental ultrasound image representing a 20×30 mm (axial×lateral) homogenous tissue. Seven artificial compressions were simulated using different compression angles (γ) and offsets (δ). The motion estimation method described in section 2.2 was employed to

track the motion between the eight resulted images. Figures 3(a) and 3(b) show the results given by the approach presented in 2.3 versus the true values of γ and δ along the image sequence. Moreover, these results are compared with those obtained by the same orientation detection, but after tracking the motion with a classical block matching method. We observe that in this case the gap between estimated and true values is larger than with our motion estimation method. In figure 3(c) we show the mean square error obtained when fitting the first order polynomial function, giving γ and δ, to measured data from lateral displacements.

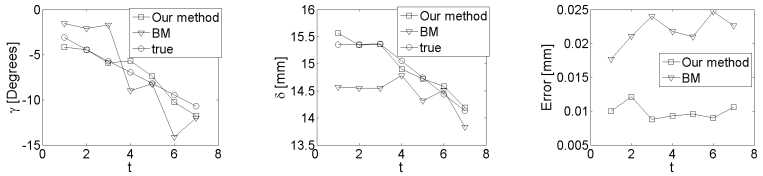

(a) (b) (c)

Figure 3. Compression orientation angle (a) and offset (b) detected using motion estimation processed with our method and with classical block matching (BM) versus true values, mean square error between first order polynomial function and data measured from lateral displacement estimated with our method and with block matching method (c).

4. EXEPERIMENTAL RESULTS

In-vivo testing of this method was performed on the sets of clinical strain images (eleven frames each) of the patients with thyroid cancer. The ultrasound acquisition was made using a clinical ultrasound scanner (Sonoline Elegra) and a 7.5-MHz linear probe (both, Siemens Medical Systems, Issaquah, XA, USA). The images were acquired while a small compression was applied to the neck over the examined medium. The contours of the thyroid gland and of the tumor on the ultrasound images were manually outlined by the radiologist who performed the examination.

Motion estimation between the ten consecutive pair of frames was processed using the algorithm presented in section 2.2. The compression orientation parameters were then calculated for each estimation result and are plotted in figures 4(a) and (b).

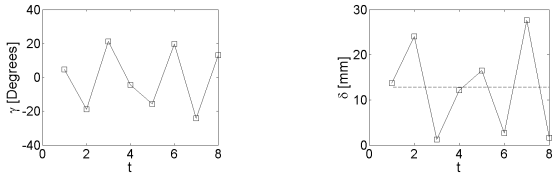

(a) (b)

Figure 4. Compression orientation angle (a) and offset (b) estimated with the thyroid image sequence.

As explained in the algorithm description at step 16, we use this compression orientation as a criterium to eliminate some of the estimation results. Note that a perfect axial compression correspond to an angle of zero degrees and to an offset equal to half the width of the processed zone, corresponding to 12.9 mm in this case (dashed line in figure 3(b)). We observe in figure 3 (b) that only three instants are close to this value, for *t* equal to 1, 4 and 5. Moreover we observe that the compression angle for the fourth and the fifth estimations are roughly the same, which is not the case for the estimation number one. For these reasons, the vector *T* introduced in step 9 and used in equation (5) (section 2.2) is set to *[4 5]* for this image sequence.

The estimation results are shown in Figure 5. Figure 5(a) shows the contours drawn by the doctor superimposed to the estimated region. Note that the estimation was processed only on a region of the images, centered to the thyroid gland. Classical strain images (axial derivate of the axial displacement) and maps of the parameter introduced in (6) are shown in Figure 5. In both cases two results are given, using the entire sequence (figures 5(d) and (f)) and using only the two selected estimations (figures 5(c) and (e)). Figure 5(b) represents the 2-D estimated motion vectors resulting from estimations 4 and 5.

As with this sequence the applied compression is never axial (the orientaion angle is always different of 0 degrees), the axial strain images are not well adapted to detect the tumor. However, on the maps representing the ratio between lateral and axial displacements the tumor is clearly visible. Note that this ratio is related by tangent function to the angle of motion vectors. In fact, it is shown in the literature that the malignant tumors are roughly five times harder than the thyroid [8]. It results that even for a non axial compression, the motion of all pixels inside the tumor is homogenous. For this reason, the ratio between the lateral and the axial components is roughly constant and different from the rest of the thyroid. In our case, the tumor is caracterized by small values of this ratio, which correspond to small angles of motion vectors. Indeed, as the tumor is harder than the thyroid, the lateral motion inside the tumor is very small compared to the rest of the tissues.

In addition, we observe that considering estimations corresponding to similar compression orientations makes the tumor be characterized by more regular and distinct margins.

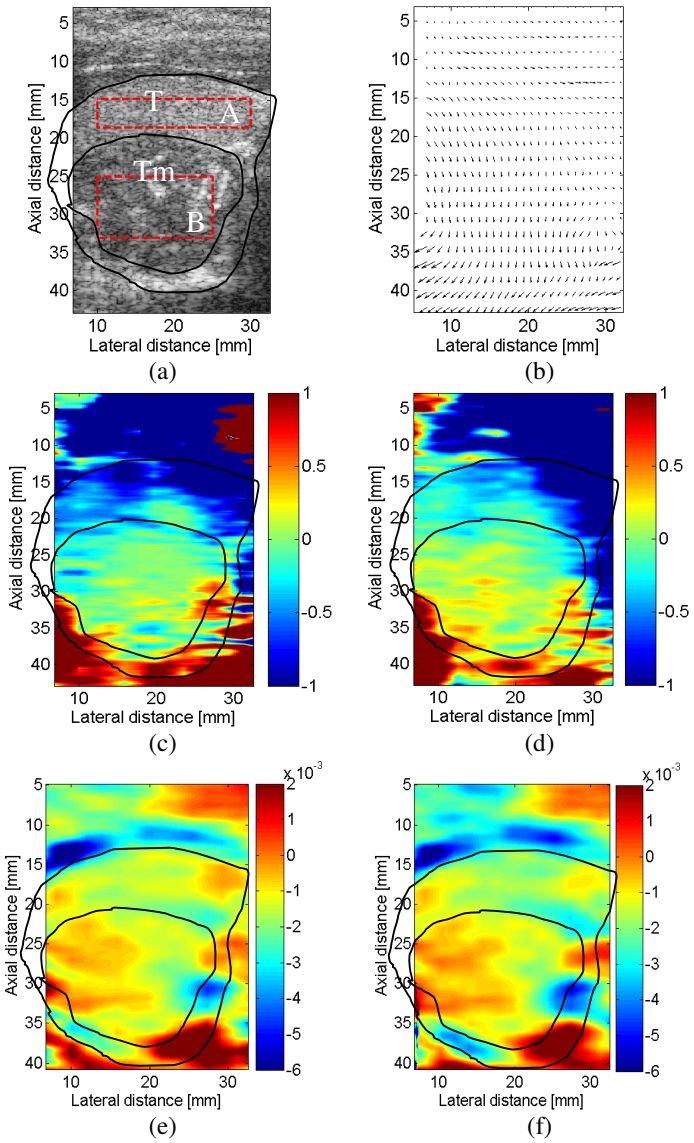

Figure 5. Estimated region, T – thyroid gland, Tm - tumor (a), estimated motion vectors (b), motion ratio map with displacements 4 and 5 (c) and with the entire sequence (d), strain images with displacements 4 and 5 (e) and with the entire sequence (f).

In figure 5(a), two rectangular regions (dashed line) are selected inside the healthy (A) and diseased (B) parts of the thyroid. For these two regions, the contrast to noise ratio (9) for B-mode images and for all estimated maps is given in table 1.

$$CNR = \frac{\mu_A - \mu_B}{\sigma_A + \sigma_B} \qquad (9)$$

where μ represents the mean value and σ the standard deviation calculated for regions A and B. We notice that the best contrast between healthy thyroid and tumor is given by the motion ratio map after images selection. The CNR is in this case roughly three times higher than with B-mode images.

B-mode	Whole sequence		T=[4 5]	
	Strain image	Motion ratio	Strain image	Motion ratio
0.53	0.6	1.19	0.23	1.6

Table 1. CNR calculated for regions A and B for B-mode image and for strain and motion ratio maps.

5. CONCLUSION

In this paper, we presented the multi-frame extension of a parametric deformable block matching adapted to ultrasound images. The method was developed for elastography and applied to thyroid cancer imaging. An approach of estimating the orientation of the applied compression is proposed. It is used to sort the acquired sequence and to calculate the final global motion of the sequence by using only accepted frames. Finally, a new parameter related to the angle of motion vectors is presented. It is shown that this parameter may improve the quality of thyroid elastograms and facilitate the thyroid cancer diagnosis.

6. REFERENCES

[1] Y. Noguchi, J. Furukawa, and H. Kiya, "Fast full search block matching algorithm for MPEG-4 videa", *IEEE ICIP*, vol. 1, pp. 61-65, 1999.

[2] J. Ophir, I. Céspedes, H. Ponnekanti, Y. Yazdi and X. Li, "Elastography : a quantitative method for imaging the elasticity of biological tissues", *Ultrasonic Imaging*, pp. 111-134, 1991.

[3] A. E. Siperstein, O. H. Clark, *Thyroid Diseases: Tumors. Carcinoma of Follicular Epithelium. Surgical Therapy, Braverman LE, Utiger RD*, eds. Werner and Ingbar's The Thyroid A Fundamental and Clinical Text. 8th ed. Lippincott Williams & Wilkins, 2000, pp. 898-899.

[4] F. Yeung, S. F. Levinson, D. Fu and K. J. Parker, "Feature-adaptive motion tracking of ultrasound image sequences using a deformable mesh", *IEEE Transactions on Medical Imaging*, vol. 17, n°6, pp.945-956, 1998.

[5] Y. Zhu, P. Chaturvedi, M. F. Insana, Strain imaging with a deformable mesh, *Ultrasonic Imaging*, vol. 21, n°2, pp. 127-41, 1999.

[6] A. Basarab, H. Liebgott, F. Morestin, A. Lyshchik, T. Higashi, R. Asato, P. Delachartre, A method of vector displacement estimation with ultrasound imaging and its application for thyroid nodular disease, *Medical Image Analysis*, in press.

[7] J. Revell, M. Mirmehdi, D. McNally, Computer vision elastography: speckle adaptive motion estimation for elastography using ultrasound sequences, *IEEE Transactions on Medical Imaging*, vol. 24, n°6, pp.755-766, 2005.

[8] A. Lyshchik, T. Higashi, R. Asato, S. Tanaka, J. Ito, M. Hiraoka, T. Saga, K. Togashi, Elastic moduli of thyroid tissues under compression, *Ultrasonic Imaging*, vol. 27, n°2, pp. 101-110, 2005.